

Turbulence topology behind different sections of the wind turbine blade

Vitalii Yanovych^{1,2,*}, Daniel Duda¹, Václav Uruba^{1,2}, Pavlo Kosiak^{1,2} and Vít Horáček¹

¹Power System Engineering, Faculty of Mechanical Engineering, University of West Bohemia in Pilsen, Univerzitní 22, 306 14 Pilsen, Czech Republic.

²Department of Fluid Dynamics, Institute of Thermomechanics, Czech Academy of Sciences, Dolejškova 5, 182 00, Prague, Czech Republic.

Abstract. This work aimed to investigate the turbulence characteristics behind different parts of the wind turbine blade. Airfoils S807, S813, S817, and S803, which characterize the shape of the blade at different lengths, were selected for estimation. During the experiment, the chord-based Reynolds number was 2.6×10^5 , while the angle of attack was zero. Measuring cross-sections were placed behind the trailing edge at $x/c \approx 0.2, 0.4$ and 1.0 . For the determination flow topology, we used a Hotwire anemometry with a split fiber probe 55R55 and a miniature X-wire probe 55P64. The obtained data allowed us to determine and compare the evolution of the wake behind different types of airfoils in streamwise and spanwise directions. Thus, the largest and smallest velocity deficit located behind S817 and S803 airfoils, respectively. This trend is also evident in the Normalized Reynolds shear stress distributions. Finally, we determined the spectrum and calculated the Integral length scale, the Taylor and Kolmogorov microscale of turbulent flow. According to the results, profile S817 contributes to the formation of a flow with a large scale of turbulence, while the S803 is contrary.

1 Introduction

The energy efficiency of wind turbines is a key factor in the economic evaluation of this type of renewable energy. It is clear that the general characteristics of this parameter depend on many subsystems [1]: blades, gearbox, generator, and control. Among these, the shape of the blade deserves special attention. Because the efficiency of wind energy transformation into the rotational motion of the generator strongly depends on aerodynamic characteristics of the blade. It should be noted that its overall design consists of different types of profiles that differ in the shape and size of the chord. Thus, the flow formed around the general geometry of the blade is a very complex three-dimensional phenomenon.

Over the last decade, the airfoil families commonly used for horizontal axis wind turbines have become widespread, including the NACA 44, NACA 23, NACA 63, and NASA LS [2]. But the main problem for them is the significant deterioration in aerodynamic characteristics due to the effects of roughness caused by contamination of the leading edge. To avoid this disadvantage for wind turbine blades, the National Renewable Energy Laboratory and

* Corresponding author: yanovych@kke.zcu.cz

Airfoils Inc. developed a new airfoil family (NREL) [3]. According to the developers, these blades are providing significant increases in annual energy production, better lift-to-drag ratios, and, in the case of stall-regulated rotors, the use of the more swept area for a given generator size. Despite these positive qualities, the issue of noise reduction and structural vibration caused by flow turbulence remains open.

That is why the scope of this paper is to perform a detailed experimental investigation of the airfoil shape effect on the turbulence evolution at different parts of blade. The general geometry of which was formed by the NREL airfoils.

2 Experimental setup and equipment

For analysis of turbulent flow evolution in different parts of the wind turbine blade, we chose a model geometry that consists of NREL airfoil profiles. This blade uses different types of airfoils, but only four of them were selected for our study S807, S813, S817, and S803. They are kept along the span of the blade from root to tip. A sketch of the wind turbine blade and its cross-section profiles shows in Fig.1 a). The airfoils were produced of thermoplastic filament material PLA by the 3D printer PRUSA i3. Thus, the quality of their surface roughness according to [4] was $Ra \approx 21.8 \mu\text{m}$. The manufactured airfoils had similar dimensions of chord length and span of $c \approx 100 \text{ mm}$ and of $l \cdot c^{-1} \approx 1$, respectively. But their thickness was somewhat different. Namely for S807 - $b \cdot c^{-1} \approx 0.19$, S813 - $b \cdot c^{-1} \approx 0.16$, S817 - $b \cdot c^{-1} \approx 0.17$ and S803 - $b \cdot c^{-1} \approx 0.15$.

The experiment was conducted in a low-speed open-type wind tunnel at the department of Power System Engineering, University of West Bohemia [5]. The internal dimensions of the test section were 0.3 m in height and 0.2 m in width, and its length was 0.75 m. The natural turbulence level amounted to about 0.1% in the working section input. Changing the position of the measuring point relative to the y and z axes was carried out using a traverse system.

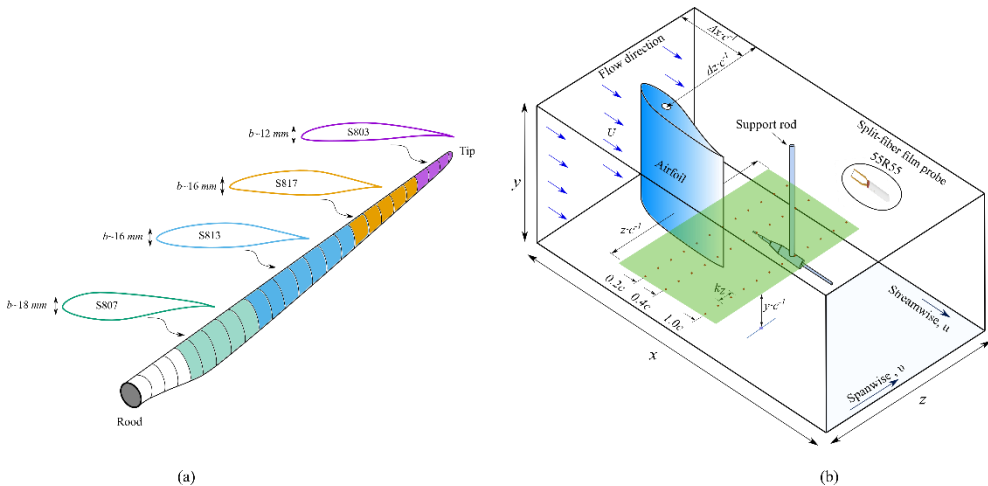


Fig. 1. a) Sketch of the wind turbine blade and its cross-section profiles. b) Airfoil model setup in the test-section and the coordinate system. The arrows in blue indicate the direction of air flow U . The green plane shows the Hot-wire measuring field. Where $z \cdot c^{-1}$, $x \cdot c^{-1}$ and $y \cdot c^{-1}$ the width, length and location height of the measuring fields, respectively. The red dots lines are a set of measuring points behind the airfoil at different cross-sections. While k_z is the distance between the measuring points. The coordinates $\Delta z \cdot c^{-1}$ and $\Delta x \cdot c^{-1}$ shows the position of the aerodynamic center of the airfoil.

Measurements were performed at zero incidence angle and at $Re \approx 2.6 \times 10^5$. The Reynolds number was based on the length of the chord. The airfoil model setup in the test section and the coordinate system are shown in Fig. 1 b). The aerodynamic center of the airfoil was located at $\Delta z \cdot c^{-1} \approx 1.9$ and $\Delta x \cdot c^{-1} \approx 2.8$. Where Δz and Δx indicate the distance between the wall and the entrance to the test section. Measurements were performed in three cross-sections from $z \cdot c^{-1} \approx -1.5$ to 1.5 at $x \cdot c^{-1} \approx 0.2, 0.4, 1.0$, and at the height $y \cdot c^{-1} \approx 1.8$. Thus the measuring field corresponded to the center of the airfoil span. The distance k_z between the measuring points was different depending on the measurement location. Thus, according to methodology [6], in the wake region $k_z \approx 3$ mm, and outside $k_z \approx 5$ mm.

Experimental studies were performed using Hot-wire anemometry and two types of probes. Namely, it was a split-fiber film probe 55R55 and a miniature X-wire probe 55P64. It should note that they allow investigation of the two-dimensional characteristics of the turbulent flow (u and v components). The split-fiber probe was used for wake topology investigation, while the wire probe for spectral and scaling analysis of vortices. In both cases, the sampling frequency and measurement time at one point were 70 kHz and 10 s, respectively. The filtering of the received signal was also applied. Namely, the High Pass filter was 10 Hz, while the Low Pass filter was 30 kHz.

3 Results and discussion

First of all, with the help of split-fiber probe 55R55, we evaluated the patterns of velocity distribution behind different types of profiles and the position of the measuring cross-section $x \cdot c^{-1}$ (Fig. 2). For convenience, the resulting curves are located relative to the position of the trailing edge at zero angle of attack and normalized by the average flow velocity U . For data analysis, we selected the range from $z \cdot c^{-1} \approx -0.5$ to 0.5 . The obtained results allowed us to evaluate the wake characteristics in streamwise and spanwise directions. In general, we can observe classical dependencies, where with increasing distance from the trailing edge, the wake depth decreases, and its width increases. According to the data, the highest and lowest velocity deficits correspond to the S817 and S803 airfoils, respectively. Especially this pattern is detected close to the trailing edge at $x \cdot c^{-1} \approx 0.2$ in a streamwise direction. Namely, under these conditions, the minimum value of $u \cdot U^{-1}$ for S817 is 13% lower than for S803. It should also note some features of the velocity distribution for S807 and S803 in the spanwise direction. The geometry of these airfoils has a more curved trailing edge than for others, which leads to some inflection of their velocity distribution at $z \cdot c^{-1} \approx 0.2$.

We also found distributions of normalized standard deviation in different measuring cross-sections behind the various types of airfoils (see Fig. 3). As we can see, the largest values of $\sigma_u \cdot U^{-1}$ and $\sigma_v \cdot U^{-1}$ are observed for the S817 profile. Moreover, the obtained graphs clearly reflect the influence of the airfoil shape on the overall distribution of the standard deviation. Namely, in the streamwise direction, the difference in the formation of double peaks of the data curve is clearly visible. That phenomenon occurs due to the vortices interactions from pressure and suction sides of the airfoil [7]. Thus, it is logical that this effect is better observed for a S813 profile with a more symmetrical profile shape. While in other cases, the flow contains mainly a single dominant structure.

The Reynolds shear stress distribution was applied to estimate of the turbulent flow anisotropy (see Fig. 4). Obtained data clearly show the range where the turbulence structure is anisotropic. Usually, it is displayed as a graphical distribution asymmetry with a combination of positive and negative numbers through the wake centerline. Thus greatest width of this range, regardless of $x \cdot c^{-1}$, is observed for S817, while the smallest one for S803 airfoil.

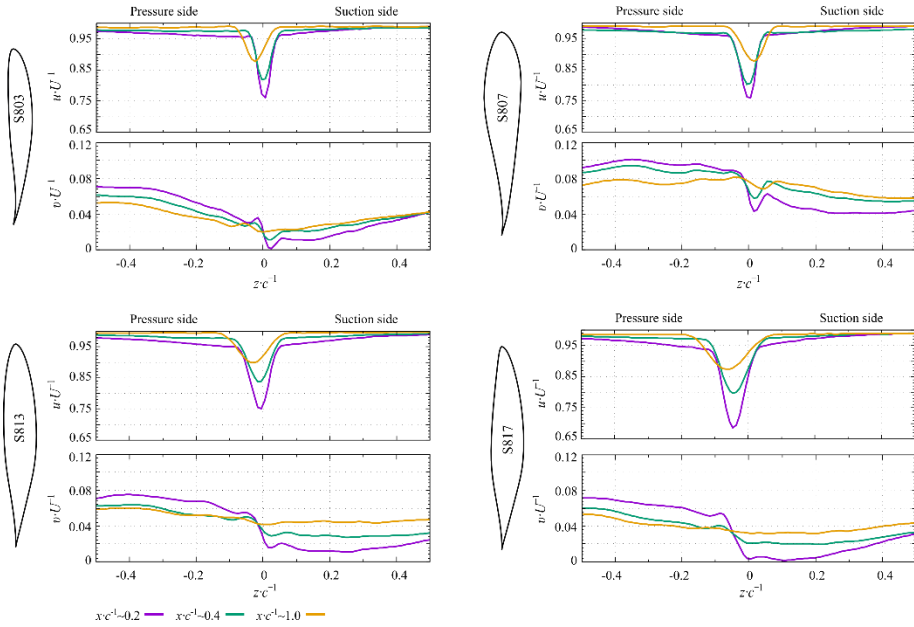


Fig. 2. The normalized profiles of streamwise $u \cdot U^{-1}$ and spanwise $v \cdot U^{-1}$ velocity components depending on the airfoil types and the distance of the measuring cross-sections $x \cdot c^{-1}$. Measurements were performed at zero incident angle and at $Re \approx 2.6 \times 10^5$. Violet, green and yellow curves characterize the position of the measuring cross-section behind the trailing edge at $x \cdot c^{-1} \approx 0.2$ and 0.4 and 1 , respectively.

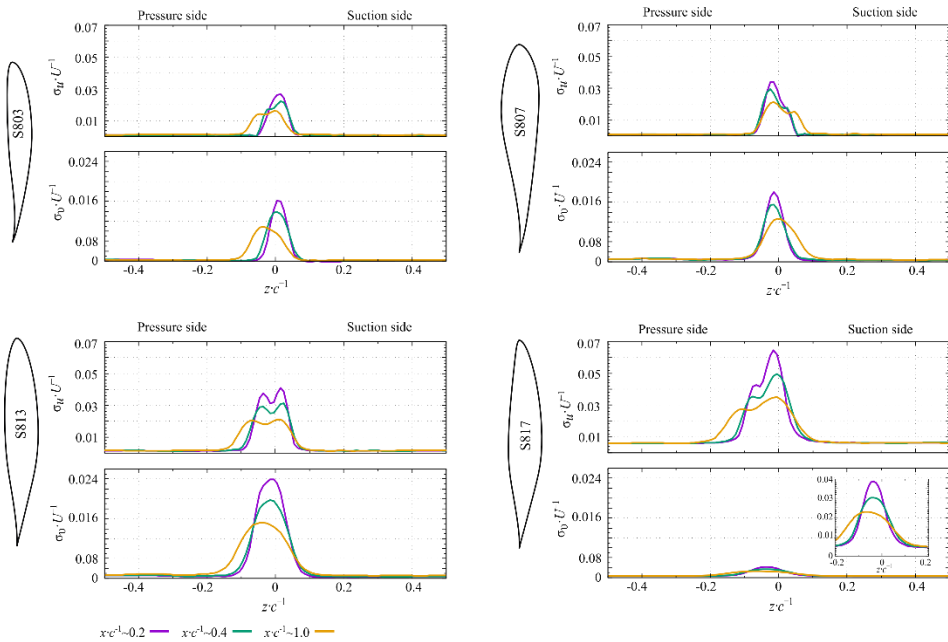


Fig. 3. Profiles of the normalized standard deviation of the streamwise $\sigma_u \cdot U^{-1}$ and spanwise $\sigma_v \cdot U^{-1}$ components depending on the airfoil types and the distance of the measuring cross-sections $x \cdot c^{-1}$. Measurements were performed at zero incident angle and at $Re \approx 2.6 \times 10^5$. Violet, green and yellow curves characterize the position of the measuring cross-section behind the trailing edge at $x \cdot c^{-1} \approx 0.2$, 0.4 and 1 , respectively.

In addition, among the entire composition of the blade, exactly these two profiles have the largest and smallest value of the Reynolds shear stress component. Accordingly to results, the magnitude of $\overline{u'v'} \cdot U^{-2}$ for S817 at $x \cdot c^{-1} \approx 0.2$ is 15 times larger than for S803.

Moreover, Fig.4 shows that the perturbation region of shear stress with a negative value is located directly on the suction side. This pattern is due to the intensity of turbulence, which increases the frictional resistance in the middle flow. As a result, turbulence receives energy, while the average flow loses. Usually, this trend is especially noticeable in the stream-wise direction. Accordingly, to Fig. 2 and Fig. 3, the highest magnitude of the velocity deficit and standard deviation was for the S817, while S803 has the opposite trend.

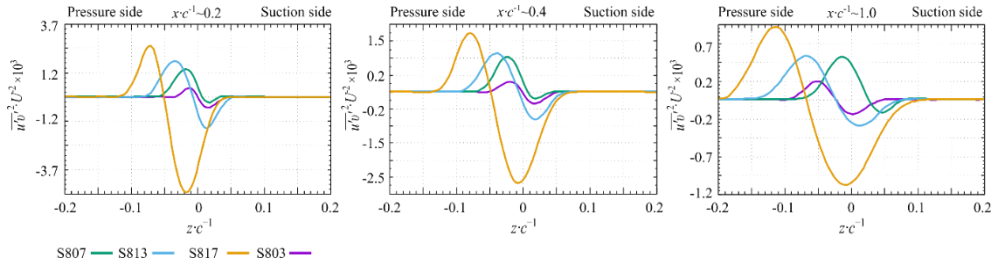


Fig. 4. Normalized Reynolds shear stress distribution at $Re \approx 1.7 \times 10^5$ depending on airfoil types and various positions of the measuring cross-sections $x \cdot c^{-1}$. Green, light blue, yellow and violet curves characterize the distributions for S807, S813, S817 and S803 airfoils respectively.

As the distance from the trailing edge increases up to $x \cdot c^{-1} \approx 1$, the shear stress decreases almost fourfold and the wake with increases almost twice. Thus, we can see some relationship between the amplitude of the Reynolds shear stress component and the energy characteristic of the vortices. According to Kolmogorov's theory [8-11], the greatest energy is contained in the largest vortices, the size of which can be described by an integral length scale L_E . To determine it, we applied the methodology well described in [12, 13]. Where the authors used correlation time series analysis to estimate the spatial scales of turbulent flows. Accordingly, the autocorrelation function for stream-wise component R_{uu} can be interpreted as:

$$R_{uu}(t) = \frac{\langle u(t+\Delta t) \cdot u(t) \rangle}{\sigma_u^2} \quad (1)$$

where the angular brackets indicate the average value u and Δt is the shift time of the signal, while $\sigma_u = \sqrt{N^{-1} \sum_{i=0}^{N-1} (u_i - \bar{u})^2}$ is standard deviation. Accordingly, N and u_i are the number of the data set, and g is the instantaneous velocity at the measurement set.

Then, using the cumulative integral of the autocorrelation function, it is easy to calculate the time scale T . That from a physical point of view interprets the average lifetime of vortices.

$$T = \int_0^{\infty} R_{uu}(t) dt \quad (2)$$

It is clear that the integral length L and time scales T are interrelated. Thus integral length can be evaluated by the equation:

$$L = T / \sigma_u \quad (3)$$

For scaling analysis, we performed measured by 55R55 probe at cross-section with coordinates $x \cdot c^{-1} \approx 1$, $y \cdot c^{-1} \approx 1.8$ and $z \cdot c^{-1}$ from -0.5 to 0.5. The obtained distributions of the integral length are shown in Fig. 5 a). As we can see, the values of the integral length scale for different types of airfoils in the spanwise direction are almost the same, where in the wake region the $L_v \approx 1.1-1.3$ mm. While in the stream-wise direction, as for the distribution of shear stresses (see Fig. 4), this parameter varies greatly. Namely, the smallest eddies are observed at S803 airfoil $L_u \approx 1.3$ mm, while the biggest at S817 are $L_u \approx 2.6$ mm. It should note that the configuration of the airfoil geometry significantly changes the evolution of the vortices. That is especially noticeable from the suction side, where the behavior of obtained distributions, in contrast to the pressure side, does not have a common trend.

After that, we analyzed the effect of the geometry of each profile on the Taylor micro-scale characteristics. From a physical point of view, that micro-scale shows the size of the vortices at which energy dissipation begins. To calculate the Taylor micro-scale, we used the classical equation:

$$\lambda = \sigma_u \sqrt{15 \cdot \nu / \epsilon} \tag{4}$$

where ν is kinematic viscosity velocity of air.

Graphical interpretation of the distribution λ depending on the type of profile shown in Fig. 5. b). Accordingly, the highest value of λ observe for S817 - $\lambda \approx 0.6$ mm, whereas the smallest one is for S803 - $\lambda \approx 0.2$ mm. The relation of these values is approximately the same in streamwise and spanwise directions.

Another important parameter of turbulent flow is the Kolmogorov microscale η . What characterizes the smallest size of vortices which cause the dissipation of kinetic energy of the flow into heat. According to paper [14], the value of η can be found from the equation:

$$\eta = (\nu^3 / \epsilon)^{1/4} \tag{5}$$

where ϵ is the dissipation rate determined by integration of the second-order structure-function and ν is kinematic viscosity of air.

Graphical interpretation of Kolmogorov microscale depending on the airfoil types is shown in Fig. 5 c).

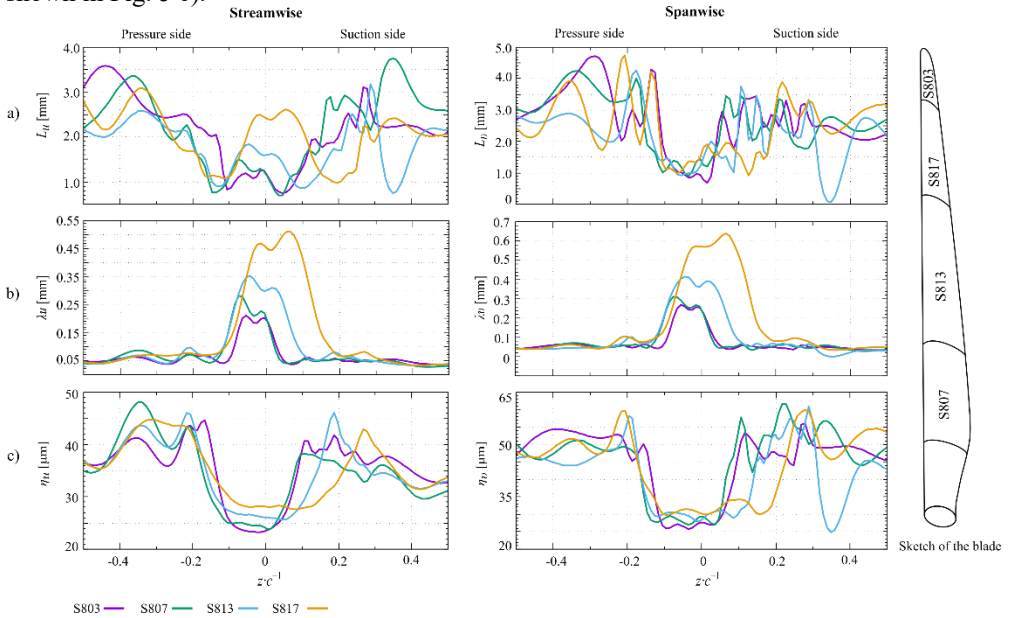


Fig. 5. Distributions of the integral length scale L , Taylor microscale λ and Kolmogorov microscale η in streamwise and spanwise directions depending on airfoils type. Measurements were carried out at $Re \approx 2.6 \times 10^5$, zero incident angle and $x \cdot c^{-1} \approx 1$. Green, light blue, yellow and violet curves characterize the distributions for S807, S813, S817 and S803 airfoils respectively.

The analysis of the obtained data revealed that regardless of the measurement direction and profile type, the value of the Kolmogorov micro-scale in the wake region does not change significantly. Thus, the maximum and minimum dimensions of the smallest vortices observe for S817 and S807. Accordingly, in both measuring directions, their values correspond to $\eta \approx 30 \mu\text{m}$ and $\eta \approx 25 \mu\text{m}$.

Power spectral density is used to estimate the distribution of flow energy between different scales of turbulence. To perform this analysis, we chose the positions of measurement points at $x \cdot c^{-1} \approx 1$, where the value of standard deviation in the streamwise direction is highest (see Fig. 3). Spectral interpretation of velocity fluctuations depending on

the airfoil types is shown in Fig. 6. Usually, according to Kolmogorov's theory [12, 13], isotropic turbulent flow is characterized by a spectral distribution with a slope of the curve in the inertial range $f = k^{-5/3}$ (see Fig. 6 a)). To better identify this range, the obtained spectrum was normalized $E(k) \cdot k^{5/3}$ and the wave number $k \cdot \eta$ (Fig. 6 b)). The obtained data show that depending on the type of profile, the width of the inertial range varies. Accordingly, we can say that the characteristics of the energy cascade, where the kinetic energy of turbulence is transmitted without loss from large scales to smaller, for different parts of the wind turbine blades change. Thus largest and smallest width of the inertial subrange is observed for S817 and S803 profiles, respectively. This pattern is manifested equally in the streamwise and spanwise directions.

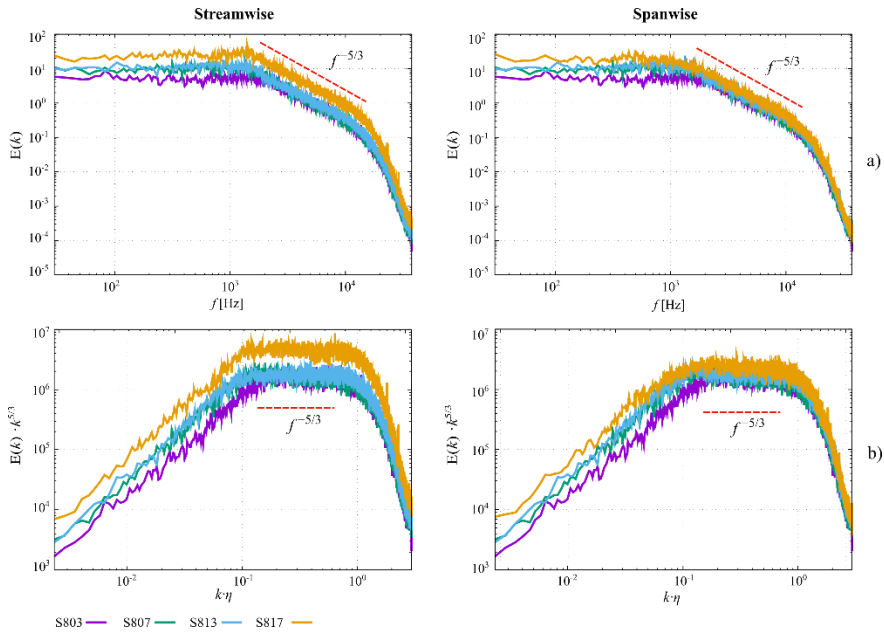


Fig. 6. Power spectral densities of stream-wise and span-wise velocity fluctuations at $Re \approx 2.6 \times 10^5$ and $x \cdot c^{-1} \approx 1$ depending on airfoils type. The upper graphs show the spectrum in the classical form, while the lower two are normalized by $k^{-5/3}$. Green, light blue, yellow and violet curves characterize the distributions for S807, S813, S817 and S803 airfoils respectively

4 Conclusion

We used Hot-wire anemometry to investigate the turbulence topology behind different parts of the wind turbine blade. Airfoil profiles S807, S813, S817, and S803, which correspond to selected parts of the blade, were selected for experimental studies. We investigated the dependence of wake parameters and turbulent flow characteristics at zero angles of attack and at the chord-based Reynolds number 2.6×10^5 . While the measuring cross-sections were placed behind the airfoil at a distance of $x \cdot c^{-1} \approx 0.2, 0.4$ and 1.0 .

Initially, using the split-fiber probe 55R55, we obtained patterns of velocity distribution and standard deviation depending on the airfoil type in the stream-wise and span-wise directions. The data show that the highest and lowest velocity deficits correspond to airfoils S817 and S803, respectively. Moreover, a similar trend persists for the standard deviation distributions.

After that, using miniature X-wire probe 55P63, we performed scaling analyses of the turbulence structure $x \cdot c^{-1} \approx 1.0$. Namely, we determined the value of the Integral length scale, the Taylor and Kolmogorov microscale in the points that correspond to the maximum values of the standard deviation. The maximum values of these parameters, regardless of the measurement direction, are observed behind S817, while the minimum is behind S803. This trend is particularly noticeable in a streamwise direction. It should be noted that there is some relationship between the behavior of the Reynolds shear stress component and the energy characteristic of vortices. Because the values of shear stress and Integral length scale vary equivalently depending on the type of profile.

Finally, we obtained the spectral power density of the flow energy distribution between different scales of turbulence for each of the profiles. The obtained graphs show that the inertial interval is the widest and narrowest for S817 and S803, respectively.

Acknowledgments

This work was financial supported by “IDEG Programme”, as part of the project Improving the Quality of Internal Grant Schemes at the University of West Bohemia in Pilsen, project reg. No. CZ.02.2.69/0.0/0.0/19_073/0016931.

References

1. N. Tenguria, N. D. Mittal and S. Ahmed. Investigation of blade performance of horizontal axis wind turbine based on blade element momentum theory (BEMT) using naca airfoils. *International journal of engineering, science and technology* **2(12)**, 25–35 (2010).
2. J. Tangler, B. Smith, D. Jager and T. Olsen. *Atmospheric Performance of the Special-Purpose SERI Thin-Airfoil Family: Final Results*, in Proceedings of the European Wind Energy Conference, 10-14 September, Madrid, Spain (1990).
3. J. Tangler and D. Somers, (1995). *NREL airfoil families for HAWT's*, report of the National Renewable Energy Laboratory (January 1995, Cole Boulevard Golden, Colorado, USA).
4. M. S. Alsoufi, A. E. Elsayed. Surface roughness quality and dimensional accuracy - a comprehensive analysis of 100% infill printed parts fabricated by a personal/desktop cost-effective FDM 3D printer. *Materials Sciences and Applications*. **09**, 11–40 (2018).
5. V. Yanovych, D. Duda, V. Horáček and V. Uruba. *Research of a wind tunnel parameters by means of cross-section analysis of air flow profiles*, in Proceedings of the Power System Engineering, AIP conference 2189, Pilsen, Czech Republic (2019).
6. V. Yanovych, D. Duda, V. Horáček and V. Uruba. *Creation of recombination corrective algorithm for research of a wind tunnel parameters* in Proceedings of the Power System Engineering, AIP conference 2118, Pilsen, Czech Republic (2019).
7. A. Zobeiri, P. Ausoni, F. Avellan, M. Farhat. How oblique trailing edge of a hydrofoil reduces the vortex-induced vibration. *Journal of Fluids and Structures* **32**, 78–89 (2012).
8. K. Choi, J. L Lumley. The return to isotropy of homogeneous turbulence. *J. Fluid Mech.* **436**, 59–84 (2001).
9. A. N. Kolmogorov, V. Levin, J. C. R. Hunt, O.M. Phillips, and D. Williams. Dissipation of energy in the locally isotropic turbulence. *Proceedings of the Royal Society of London. Series A: Mathematical and Physical Sciences* **434**, 15–17 (1991)

10. G. K. Batchelor. *The Theory of Homogeneous Turbulence* (Cambridge University Press, New York, US, 1982).
11. J. L. Lumley, G. Newman. The return to isotropy of homogeneous turbulence. *J. Fluid Mech.* **82**, 161–178 (1977).
12. M. Bourgoïn et al. Investigation of the small-scale statistics of turbulence in the modane S1MA wind tunnel. *CEAS Aeronautical Journal* **9**, 269–281 (2018).
13. V. Yanovych, D. Duda, V. Uruba. Structure turbulent flow behind a square cylinder with an angle of incidence, *European Journal of Mechanics, B/Fluids* **85**, 110–123 (2021).
14. V. Yanovych, D. Duda, V. Uruba and T. Tomášková. Hot-Wire Investigation of Turbulence Topology behind Blades at Different Shape Qualities, *Processes* **10(3)**, 522 (2022).
15. S. B. Pope. *Turbulent Flows*, 1st ed. (Cambridge University Press, New York, US, 2000).
16. P. Kundu, I. Cohen and D. Dowling. *Fluid Mechanics*. 6th ed. (Academic Press, London, UK, 2016).